

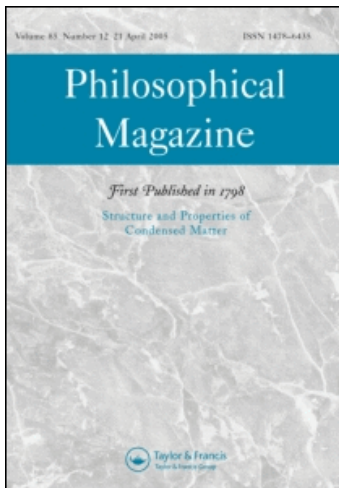
This article was downloaded by: [Stanford University]

On: 12 May 2010

Access details: Access Details: [subscription number 917394057]

Publisher Taylor & Francis

Informa Ltd Registered in England and Wales Registered Number: 1072954 Registered office: Mortimer House, 37-41 Mortimer Street, London W1T 3JH, UK



Philosophical Magazine

Publication details, including instructions for authors and subscription information:

<http://www.informaworld.com/smpp/title~content=t713695589>

***In situ* synchrotron X-ray microdiffraction analysis of thermomechanically induced phase transformations in Cu-Al-Ni shape-memory alloy**

H. -S. Zhang ^a; K. Komvopoulos ^a

^a Department of Mechanical Engineering, University of California, Berkeley, CA 94720, USA

First published on: 23 April 2010

To cite this Article Zhang, H. -S. and Komvopoulos, K. (2010) '*In situ* synchrotron X-ray microdiffraction analysis of thermomechanically induced phase transformations in Cu-Al-Ni shape-memory alloy', *Philosophical Magazine*, 90: 16, 2235 – 2248, First published on: 23 April 2010 (iFirst)

To link to this Article: DOI: 10.1080/14786431003630892

URL: <http://dx.doi.org/10.1080/14786431003630892>

PLEASE SCROLL DOWN FOR ARTICLE

Full terms and conditions of use: <http://www.informaworld.com/terms-and-conditions-of-access.pdf>

This article may be used for research, teaching and private study purposes. Any substantial or systematic reproduction, re-distribution, re-selling, loan or sub-licensing, systematic supply or distribution in any form to anyone is expressly forbidden.

The publisher does not give any warranty express or implied or make any representation that the contents will be complete or accurate or up to date. The accuracy of any instructions, formulae and drug doses should be independently verified with primary sources. The publisher shall not be liable for any loss, actions, claims, proceedings, demand or costs or damages whatsoever or howsoever caused arising directly or indirectly in connection with or arising out of the use of this material.

***In situ* synchrotron X-ray microdiffraction analysis of thermomechanically induced phase transformations in Cu–Al–Ni shape-memory alloy**

H.-S. Zhang and K. Komvopoulos*

*Department of Mechanical Engineering, University of California,
Berkeley, CA 94720, USA*

(Received 19 September 2009; final version received 17 January 2010)

Phase transformations in a single-crystal Cu–Al–Ni shape-memory alloy induced by thermomechanical effects were investigated *in situ* by high-resolution synchrotron X-ray microdiffraction. Contrary to the common belief, austenite texture maps revealed that austenite-to-martensite transformation occurred during heating of the partially transformed material under fixed specimen elongation. Twinned and detwinned types of martensite coexisted during this austenite-to-martensite phase transformation. Twinning and detwinning structures evolved to accommodate changes in stress and strain generated in the temperature-varying environment. Small amounts of austenite exhibiting distorted crystallographic orientation were detected in regions of stress-induced martensite during heating of the partially transformed material. The results of this investigation provide insight into intriguing stress rate-dependent phenomena intrinsic of shape-memory alloys and elucidate complex phase transformations due to thermal and mechanical stress effects.

Keywords: austenite; elongation; martensite; phase transformation; shape-memory alloy; strain; stress; synchrotron radiation; thermomechanical effects; twinning; X-ray diffraction

1. Introduction

The high elastic strain and shape-memory effect resulting from reversible phase transformations involving multiple austenite and martensite phases make shape-memory alloys (SMAs) important functional materials. Because austenite-to-martensite phase transformation in SMAs is normally observed with a temperature decrease, austenite and martensite are referred to as high- and low-temperature phases, respectively. Austenite-to-martensite phase transformations can also be induced by mechanical stresses.

Despite significant insight into phase transformations obtained from *ex situ* observations [1–27], *in situ* investigations and basic understanding of phase changes in SMAs due to simultaneous thermal and mechanical stress effects are sparse.

*Corresponding author. Email: kyriakos@me.berkeley.edu

Temperature changes during deformation of a SMA may significantly affect the stress–strain response. For example, heating (cooling) of partially transformed Cu–Al–Ni and Ti–Ni alloys under uniaxial tension has been reported to lead to a rapid increase (decrease) in stress [18–20]. Therefore, *in situ* tracking of phase transformations is essential for studying the effect of temperature changes on the mechanical response of SMAs.

Synchrotron X-ray microdiffraction is a powerful method for *in situ* studies of nucleation and growth mechanisms controlling phase transformations in SMAs. The unique capability of this method relies on texture and strain maps of micrometer resolution that enable *in situ* observation of microstructure changes over a relatively large sample area [28–35]. Synchrotron X-ray microdiffraction combines high-resolution X-ray source, focusing optics, large-surface-area/fast-detector technology, and software for Laue pattern analysis. Although the microstructures of various SMAs have been characterized by this technique in previous studies [31–37], the present investigation is the first to reveal an unexpected austenite-to-martensite phase transformation during heating of a SMA under constant elongation.

Single-crystal Cu–Al–Ni alloy was selected for study because of its unique potential to accommodate the largest recoverable strain ($\sim 17\%$) among all SMAs. Moreover, this alloy exhibits high thermal and electrical conductivity, temperature-dependent damping ratio [2,11,38], and can be fabricated in large single crystals, which is convenient for *in situ* texture analysis in a thermomechanical environment. The large strain recovery and tunable damping ratio are attributed to four martensite phases (α'_1 , β'_1 , β''_1 , and γ'_1) produced from austenite (β_1) under different stress and temperature environments. Transformations between these phases can be associated with variations in temperature and applied stress [1–9]. For example, γ'_1 is observed at temperatures below or close to the phase-transformation temperature [3,4,8,9], whereas β''_1 evolves during deformation of γ'_1 [1,2,5]. Because the temperature was maintained well above the phase-transformation temperatures, only two martensite phases (α'_1 and β'_1) could coexist with austenite β_1 in the present study. Austenite texture and strain maps obtained by *in situ* synchrotron X-ray microdiffraction are presented to elucidate the evolution of austenite-martensite phase transformations in Cu–Al–Ni alloy under conditions of heating and uniaxial tensile loading and unloading.

2. Experimental procedures

2.1. Specimens

Single-crystal Cu–Al–Ni alloy rods of 6.35 mm diameter were fabricated from a molten pool of 82 Cu, 14 Al, and 4 Ni (all wt.%) using the Czochralski method. The rods were first heated to $\sim 870^\circ\text{C}$ and then quenched to acquire austenite microstructures. The room-temperature microstructure of Cu–Al–Ni alloy is cubic austenite (DO_3 microstructure), and the phase transformation temperatures are below -30°C [18]. Dog-bone shape tensile specimens of 0.15 mm thickness (Figure 1) were fabricated from the austenite rods by electrical discharge machining. In all of the experiments, the stretching direction (x -direction) of the specimen was along the [001] austenite crystallographic orientation.

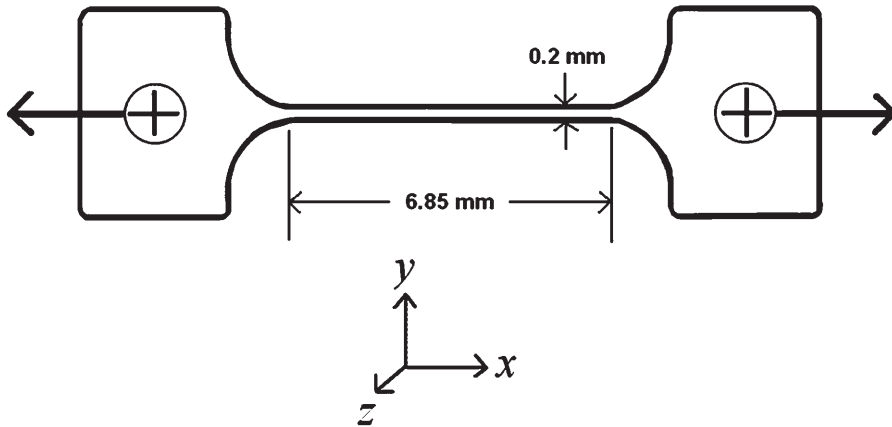


Figure 1. Schematic of tensile specimen used in the thermomechanical stretching experiments. The specimen was fastened onto the tensile jig by two screws with washers through the holes at the two ends. Arrows indicate the stretching direction.

2.2. Synchrotron X-ray microdiffraction setup

A custom-made elongation-control tensile jig was mounted onto the synchrotron microdiffraction stage. The specimen was heated with an electrical heating cartridge (HDC19100, Tempco, IL) connected to the specimen by a metal bar, whereas the microdiffraction stage and tensile jig were continuously cooled by cold nitrogen gas. The temperature was measured with a thermocouple attached to the specimen. Stress and strain measurements were not affected by temperature variations because the jig frame was maintained at a low temperature. The movement of the specimen stage was controlled to an accuracy of less than $1\ \mu\text{m}$. The elongation of the specimen was measured with an optical microscope mounted onto the microdiffraction stage and the force exerted to the specimen by a load cell. The engineering stress and strain were calculated from the measured force and elongation, respectively. In the experiments where the temperature of the specimen was increased, the load cell measured the net force under the simultaneous effects of the microstructure evolution and thermal expansion. Before testing, the specimen was stretched a few times to stabilize the system.

The high spatial resolution ($\sim 1\ \mu\text{m}^2$) of the 12.3.2 X-ray microdiffraction beamline (formerly 7.3.3) at the Advanced Light Source [28–30,36] (Lawrence Berkeley National Laboratory, Berkeley, CA) enables *in situ* observation and analysis of microstructure changes during thermomechanical deformation. Roughness features at the specimen edges (detected by fluorescence scanning) were used to track the analysis area on the specimen surface during the experiment. By combining optical microscopy and fluorescence scanning, the analysis area was located to a precision of $\sim 1\ \mu\text{m}$. Polychromatic (5–22 keV) Laue diffraction patterns were obtained with a beam radius equal to $\sim 1\ \mu\text{m}$. In all texture maps, regions not indexed by the austenite microstructure are shown in black. The details of the mathematical algorithms for computing strain and crystallographic orientation matrixes from

Laue patterns can be found elsewhere [29,37]. Because the Cu–Al–Ni alloy was in its single-crystal form (i.e. continuous crystal lattice without grain boundaries) and the sampling depth in the X-ray diffraction measurements was equal to several micrometers (i.e. about three orders of magnitude larger than the lattice constant (0.58 nm) of the material [2,9]), the results are representative of the bulk behavior. Phase maps were obtained by analyzing more than 10,000 Laue diffraction patterns collected for several days in a grid matrix. This involved the acquisition of tens of gigabytes of data and months of computational analysis with a Dell Precision PWS-690 workstation having a 2.33 GHz Intel processor and 4 GB RAM.

3. Results

3.1. Thermomechanical behavior of Cu–Al–Ni alloy

Figure 2 shows a representative stress–strain response of single-crystal Cu–Al–Ni alloy for a maximum elongation of $\sim 13\%$. The initial small stress (point A) is due to slight stretching of the specimen to stabilize the system before testing. The loading and unloading paths (ABCD and DEA, respectively) reveal a fully reversible deformation at 25°C , indicating the recovery of the austenite phase upon unloading. The initial portion of the loading curve reflects the elastic response of the austenite β_1 phase. A maximum elongation of $\sim 1.5\%$ was accommodated in the austenite lattice without atomic shuffling. Specimen stretching to an elongation above 1.5% produced a stress plateau characteristic of the austenite–martensite ($\beta_1 \rightarrow \beta'_1$) phase transformation [5–8]. Further stretching up to $\sim 7.5\%$ elongation (point C) led to the completion of $\beta_1 \rightarrow \beta'_1$ transformation by a nucleation and growth process accompanied by a slight stress increase. The stress plateau corresponding to the

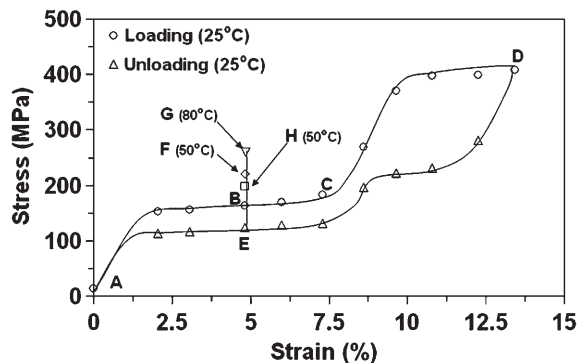


Figure 2. Stress–strain response of single-crystal Cu–Al–Ni shape-memory alloy. The loading–unloading cycle ABCDEA was obtained at room temperature (25°C). Points F and G were obtained by stretching the specimen up to an elongation of $\sim 5\%$ at 25°C (point B) and then heating to 50 and 80°C , respectively, while maintaining the specimen at a constant elongation of $\sim 5\%$. Point H was obtained by unloading the specimen from a maximum elongation of $\sim 13\%$ (point D) to an elongation of $\sim 5\%$ (point E) at 25°C and then heating to 50°C , while maintaining the specimen at a constant elongation of $\sim 5\%$.

austenite-martensite phase change is typical of most SMAs. The sharp stress increase beyond point C indicates the saturation of $\beta_1 \rightarrow \beta'_1$ phase change. The linear elastic response after point C is characteristic of the deformation behavior of the β'_1 phase. A second stress plateau associated with martensite-martensite ($\beta'_1 \rightarrow \alpha'_1$) phase transformation [1,2,5,10] was encountered when the specimen elongation was increased above $\sim 10\%$. Unloading from a maximum elongation of $\sim 13\%$ (point D) produced a stress hysteresis. The first and second stress plateaus of the unloading path are attributed to reverse martensite-martensite ($\alpha'_1 \rightarrow \beta'_1$) and martensite-austenite ($\beta'_1 \rightarrow \beta_1$) phase transformations, respectively, whereas the three stress decreases reflect the elastic responses of $\beta'_1 + \alpha'_1$, β'_1 , and β_1 phases. These sequential phase changes resulted in the full recovery of a maximum tensile strain of $\sim 13\%$, illustrative of the remarkable superelastic behavior of single-crystal Cu-Al-Ni alloy.

Heating of the partially transformed material (point B) to 50°C (point F) and then to 80°C (point G) while keeping the elongation fixed at $\sim 5\%$ resulted in a dramatic stress increase. The same trend was observed during unloading. When the partially transformed material (point E) was heated to 50°C (point H) under a fixed elongation of $\sim 5\%$, the stress increased sharply. Thermal expansion due to heating produced a compressive stress; however, the net stress change (represented by BF, FG, and EH) is tensile, suggesting the development of a much higher tensile stress due to the microstructure evolution. Thus, a sharp tensile stress increase resulted from heating the specimen under fixed elongation during $\beta_1 \rightarrow \beta'_1$ (loading) and $\beta'_1 \rightarrow \beta_1$ (unloading) phase transformation.

3.2. In situ synchrotron X-ray microdiffraction of Cu-Al-Ni alloy under isothermal loading

Figure 3 shows austenite texture maps obtained before and after $\beta_1 \rightarrow \beta'_1$ phase transformation (points A and C, respectively) that provide information about the austenite crystallographic orientation. Since the stress-strain response (Figure 2) revealed that specimen stretching up to a maximum elongation of $\sim 13\%$ did not yield residual deformation (i.e. fully reversible austenite-to-martensite phase change), the black regions in the texture maps are assigned to martensite. Martensite cannot be revealed by polychromatic diffraction because the lath structure of transformed martensite is smaller than the X-ray beam size [36]. Therefore, only austenite was indexed and color-coded according to its crystallographic orientation (Miller index) using the specimen (global) coordinates as a reference system (Figure 1). Figures 3a-3c show that the undeformed (as-fabricated) microstructure (point A) consists of austenite with a uniform crystallographic orientation, consistent with the room-temperature microstructure of single-crystal austenite. The few non-austenitic (black) regions in these texture maps are associated with crystal defects and/or tiny amounts of retained martensite produced from stretching of the specimen before testing to stabilize the system. Figures 3d-3f show that elongation up to $\sim 7.5\%$ (point C) increased dramatically the area of the black regions, indicating the occurrence of $\beta_1 \rightarrow \beta'_1$ phase transformation. Retained austenite in the form of randomly dispersed microdomains can also be observed in the texture maps shown in Figures 3d-3f; however, its crystallographic orientation differs from that of the

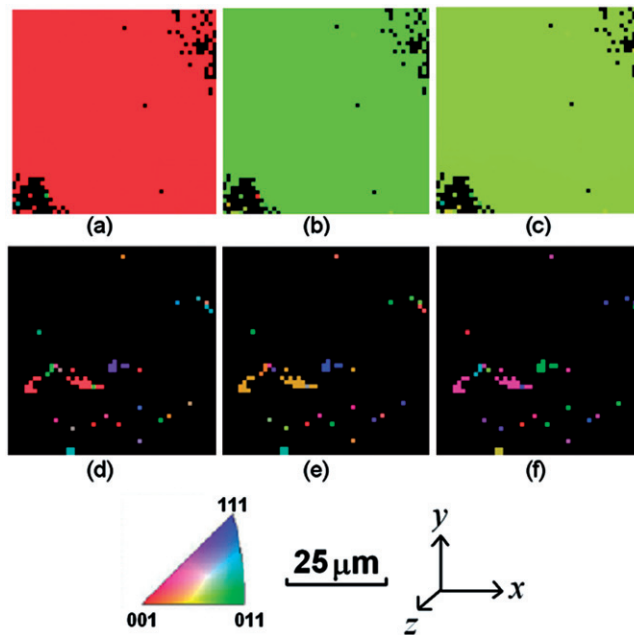


Figure 3. Austenite texture maps ($1 \times 1 \mu\text{m}^2$ grid size) of microstructures corresponding to points A and C of the stress-strain response shown in Figure 2. The x -, y -, and z -direction maps of points A and C are shown in (a)–(c) and (d)–(f), respectively.

original austenite (Figures 3a–3c), presumably due to the effect of austenite/martensite interface stresses.

X-ray microdiffraction was also used to obtain insight into the deformation of austenite. Six strain components are needed to determine the strain at a material point, i.e. ε_{xx} , ε_{yy} , and ε_{zz} normal strains in the x -, y -, and z -directions and ε_{xy} , ε_{xz} , and ε_{yz} shear strains on the (x,y) , (x,z) , and (y,z) planes, respectively. The complete strain information of the austenite phase in the microstructure corresponding to point C is given by the maps shown in Figure 4. The strain maps reveal the existence of dispersed austenite microdomains that exhibit complex tensile, compressive, and shear deformation. Earlier synchrotron studies have also shown that retained austenite in stress-induced martensite regions is under a state of stress [32,37]. The distortion of the austenite microdomains due to the anisotropic multiaxial stress introduced by surrounding martensite domains is attributed to atom bond continuity across martensite/austenite boundaries.

3.3. In situ synchrotron X-ray microdiffraction of Cu–Al–Ni alloy under thermo-mechanical loading

To examine thermomechanically induced phase transformations in Cu–Al–Ni alloy, X-ray microdiffraction analysis was performed *in situ* while the elongated specimen

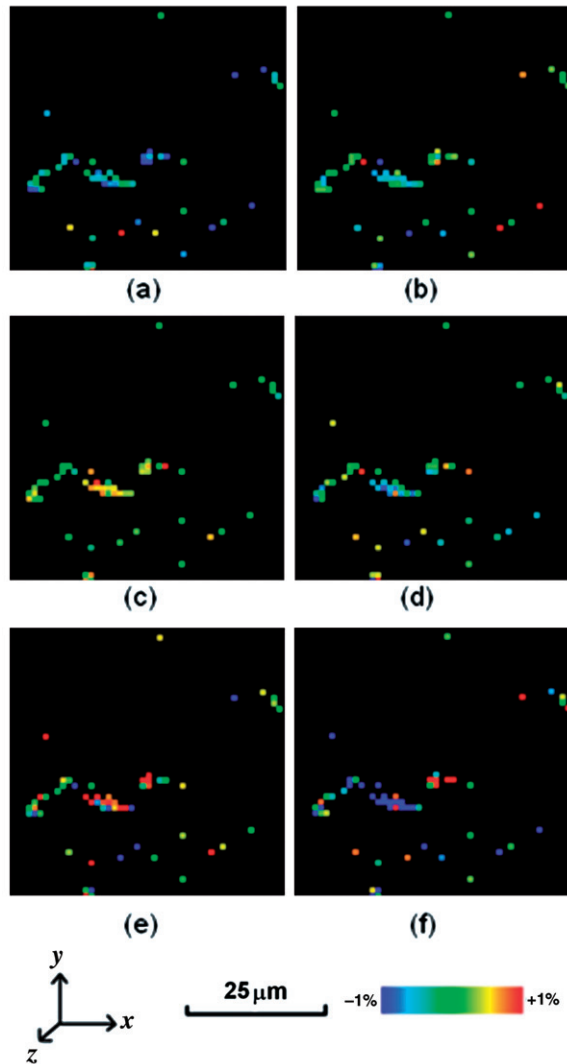


Figure 4. Strain maps ($1 \times 1 \mu\text{m}^2$ grid size) of microstructure corresponding to point C of the stress-strain response shown in Figure 2: (a) ε_{xx} , (b) ε_{yy} , (c) ε_{zz} , (d) ε_{xy} , (e) ε_{xz} and (f) ε_{yz} .

was heated at different temperatures. Figure 5 shows austenite texture maps corresponding to the microstructures of characteristic points of the thermomechanical response shown in Figure 2. The maps shown in Figures 5a–5c illustrate the partial evolution of $\beta_1 \rightarrow \beta'_1$ phase transformation and the existence of untransformed (original) austenite regions of fairly uniform crystallographic orientation (point B). Domains of retained austenite are dispersed in stress-induced martensite regions and are highly distorted, as in the microstructure of point C.

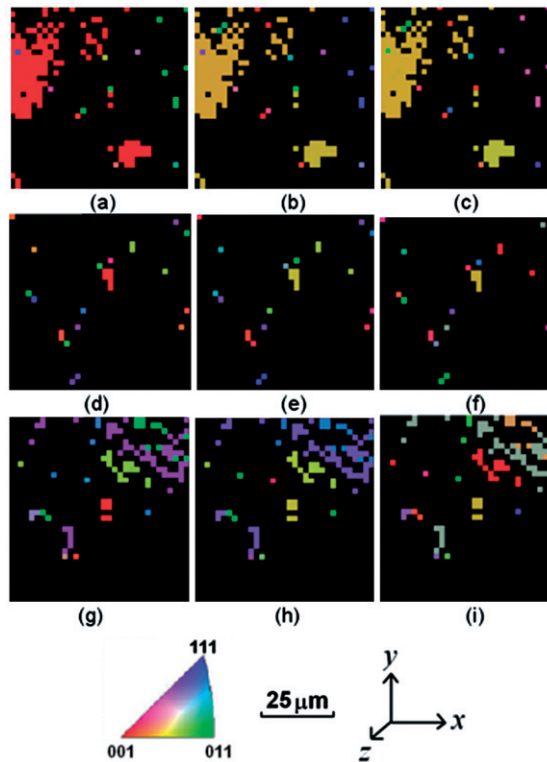


Figure 5. Austenite texture maps ($1.5 \times 1.5 \mu\text{m}^2$ grid size) of microstructures corresponding to points B, F, and G of the stress–strain response shown in Figure 2. The x -, y -, and z -direction maps of points B, F, and G are shown in (a)–(c), (d)–(f), and (g)–(i), respectively.

The texture maps corresponding to point F (Figures 5d–5f) indicate that heating to 50°C while keeping the elongation fixed at $\sim 5\%$ yielded some intriguing phenomena. First, some austenite microdomains with crystallographic orientations distinctly different from that of the original austenite are shown to be randomly dispersed in stress-induced martensite regions. Second, untransformed austenite regions in Figures 5a–5c are shown as black regions in the maps of Figures 5d–5f. Because of fully reversible deformation (Figure 2), plastic deformation is precluded as a possible source of this phenomenon. Thus, the disappearance of untransformed austenite from the texture maps of Figures 5d–5f is attributed to austenite-to-martensite transformation. This is contrary to the common belief that austenite is the high-temperature phase and that heating leads to martensite-to-austenite transformation. The further increase of the temperature to 80°C (point G in Figure 2) caused some martensite to transform to austenite (Figures 5g–5i). The texture of the thermally induced austenite also differs significantly from that of the original austenite. Since point G has the highest temperature in Figure 2, the majority of the austenite in this microstructure resulted from heating from 50°C (point F) to 80°C (point G). Strain maps of the

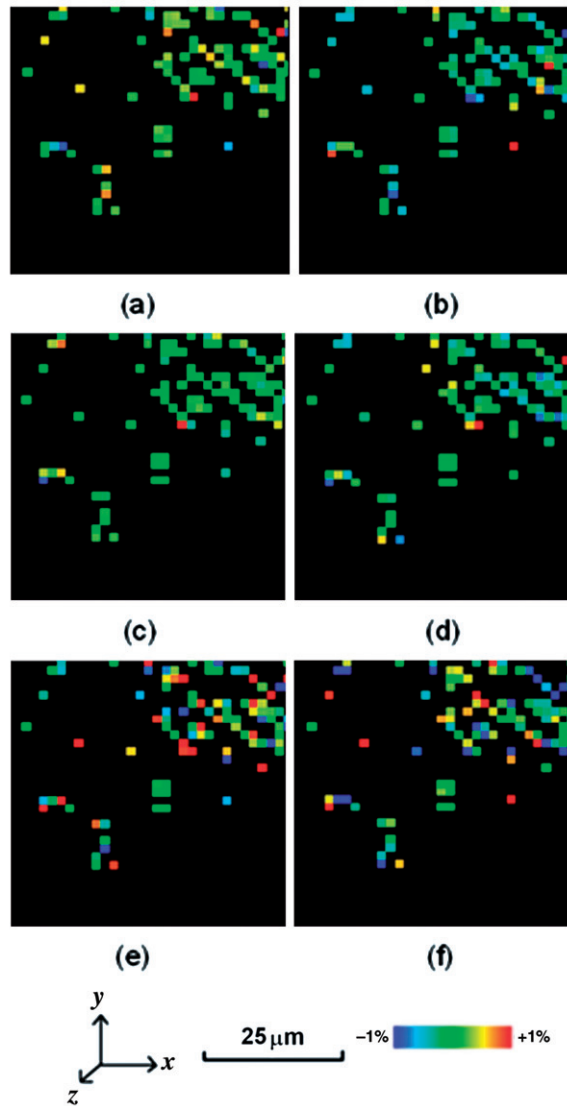


Figure 6. Strain maps ($1.5 \times 1.5 \mu\text{m}^2$ grid size) of microstructure corresponding to point G of the stress–strain response shown in Figure 2: (a) ε_{xx} , (b) ε_{yy} , (c) ε_{zz} , (d) ε_{xy} , (e) ε_{xz} and (f) ε_{yz} .

microstructure corresponding to point G, shown in Figure 6, reveal randomly distorted austenite domains, similar to those of retained austenite in the microstructure of point C (Figure 4).

Such counterintuitive austenite-to-martensite transformation induced by heating under fixed elongation was also observed during unloading, as evidenced by the austenite texture maps of microstructures corresponding to point E (Figures 7a–7c) and point H (Figures 7d–7f) of the unloading response. The decrease in the amount

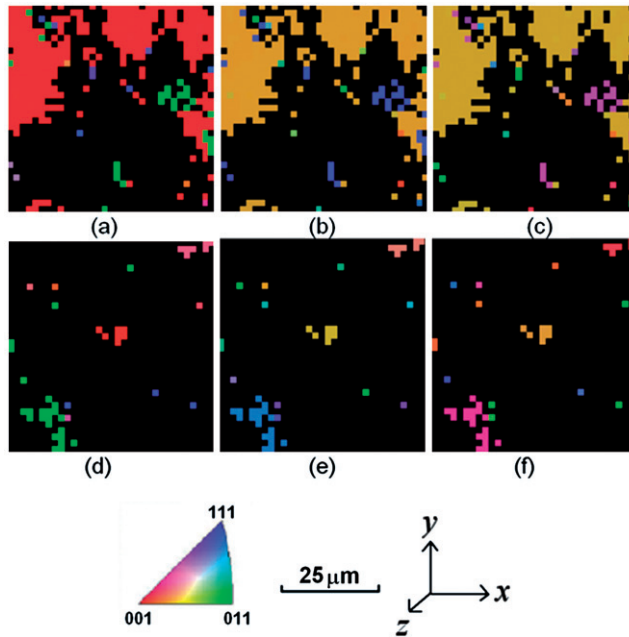


Figure 7. Austenite texture maps ($1.5 \times 1.5 \mu\text{m}^2$ grid size) of microstructures corresponding to points E and H of the stress–strain response shown in Figure 2. The x -, y -, and z -direction maps of points E and H are shown in (a)–(c) and (d)–(f), respectively.

of original austenite and the formation of dispersed austenite microdomains during heating under fixed elongation were also observed in X-ray microdiffraction scans of larger specimen areas (e.g. $200 \times 200 \mu\text{m}^2$) and different elongation levels (e.g. $\sim 2.5\%$ strain).

4. Discussion

Twinning and/or detwinning inevitably occurred in the martensite phase due to the cubic austenite and monoclinic martensite phases of Cu–Al–Ni alloy. Such cubic-to-monoclinic structure transformation and twinning/detwinning are characteristic of most SMAs. Martensite microstructures of the same crystallographic orientation form zones known as variants. Under uniaxial tension, austenite can transform to multi-variant (twinned) martensite; however, only one variant dominates martensite growth by detwinning to accommodate the elongation in the stretching direction [6,34,39–41]. The superelastic behavior of SMAs is due to detwinned (single-variant) martensite, which is formed without breaking the original atomic bonds. The strain due to martensite detwinning (Bain strain) can be determined from a crystallography analysis for fixed austenite crystallographic direction. For example, stretching austenite along the [001] direction induces $\beta_1 \rightarrow \beta'_1$ phase transformation in Cu–Al–Ni alloy, resulting in a reversible strain of

~8.5% [1,2,6,9–11]. However, twinned martensite does not contribute to the overall strain because the variants maintain the original macroscopic shape by a self-accommodation mechanism [27]. Partially transformed microstructures of Cu–Al–Ni alloy, such as those of points B and E, are mixtures of austenite and martensite, as shown in Figures 5a–5c and Figures 7a–7c, respectively. To accommodate the global deformation at a given elongation (strain), the fraction of detwinned martensite must be fixed regardless of the applied thermomechanical stress. Alternatively, different fractions of twinned martensite could be encountered at a given strain. For example, although points E, B, H, F, and G have the same elongation (~5%), the microstructures corresponding to points E and F exhibit the lowest and highest martensite fractions, respectively, as indicated by the texture maps shown in Figures 5 and 7. This difference is attributed to the formation of twinned martensite.

For both isothermal and temperature-varying conditions, phase-transformation stresses of SMAs show a dependence on temperature. In particular, the austenite-martensite phase-transformation stress increases with temperature [4,18,22,23,26]. The ratio of the change in phase-transformation stress to the temperature change is known as stress rate. Stress rate-dependent phenomena can be associated with austenite-martensite interfaces and martensite variant boundaries. The increase in temperature exacerbates atomic structure incompatibilities across phase interfaces and variant boundaries, resulting in a higher macroscopic stress [18]. Phase interfaces and variant boundaries can exist under different conditions. For instance, martensite variant boundaries have been observed even after saturation of the detwinning process induced by an increase in macroscopic deformation [16–18]. Moreover, retained austenite preserves austenite/martensite interfaces. The higher stresses at austenite/martensite interfaces and martensite variant boundaries produced from heating may contribute to the driving force for gross transformation of the original austenite to martensite under fixed elongation (strain). Heating of stress-induced martensite resulted in limited reverse transformation to austenite, as evidenced by the existence of randomly dispersed austenite microdomains (Figures 5 and 7). Although such austenite transformation is mainly due to the temperature increase, anisotropic thermal expansion of martensite domains might have also played a contributing role. Despite the small amount of such reverse transformation, the effect on the rest of the material was significant because it increased the density of austenite/martensite interfaces. Moreover, such reverse transformation in detwinned martensite regions may induce elongation incompatibility due to differences in length between detwinned martensite and austenite in the stretching direction. Such elongation incompatibility may also enhance austenite-martensite transformation during heating. For the macroscopic shape to be maintained by the self-accommodation mechanism, martensite formed by heating must be in the twinned condition, similar to multi-variant martensite formed by cooling. The temperature rise from 50 to 80°C promoted further austenite formation in stress-induced martensite regions, increasing the austenite fraction in the microstructure of point G compared to that of point F (see Figures 5d–5i). The austenite formed by heating was distorted (Figure 6) by the interface stress applied by the surrounding martensite domains, resulting in

significant texture differences compared to the texture of the original single-crystal austenite.

The results of this study raise a question about interacting thermal and mechanical effects on the microstructure evolution in SMAs. In view of the different properties of austenite and martensite, austenite-martensite phase transformation induced by heating under fixed elongation (deformation) has important implications in the reliability and performance of SMA devices and components operating in environments of varying temperature and mechanical stresses. Therefore, the microstructure changes in single-crystal Cu–Al–Ni alloy due to mechanical and thermal effects observed in this study have direct implications in the design and endurance of SMA devices.

5. Conclusions

Phase transformation phenomena in single-crystal Cu–Al–Ni shape-memory alloy due to thermal and mechanical effects were investigated *in situ* by synchrotron X-ray microdiffraction. Based on the presented results and discussion, the following main conclusions can be drawn from this study.

- (1) During austenite–martensite transformation induced by uniaxial stretching, retained austenite was distorted by austenite/martensite interface stresses.
- (2) Small amounts of austenite microdomains dispersed in stress-induced martensite regions were produced by heating of the partially transformed material. These austenite microdomains increased with temperature and were distorted by the stress due to surrounding martensite regions.
- (3) Contrary to the common belief that austenite is the high-temperature phase in SMAs and that heating results in martensite–austenite transformation, the original austenite in the partially transformed material transformed to martensite upon heating under fixed elongation (strain). This unexpected phase transformation can be explained by stress rate-dependent phenomena associated with austenite/martensite interfaces and martensite variant boundaries.
- (4) Twinned and detwinned martensites coexist during stress-induced martensite transformation, and twinning or detwinning occurs to accommodate changes in stress and strain in the temperature-varying environment.

Acknowledgements

This work was performed at the Advanced Light Source and the Molecular Foundry, Lawrence Berkeley National Laboratory, supported by the Office of Science, Office of Basic Energy Sciences, US Department of Energy, under Contract No. DE-AC02-05CH11231. The microdiffraction beamline 12.3.2 has been partially funded by the National Science Foundation under Grant No. 0416243. The authors acknowledge discussions with R. Ritchie, R. Gronsky, A. Pelton, M. Barney and S. Robertson, and technical assistance by N. Tamura and M. Kunz.

References

- [1] K. Otsuka, H. Sakamoto and K. Shimizu, *Acta Metall.* 27 (1979) p.585.
- [2] H. Funakubo, *Shape Memory Alloys*, Translated from the Japanese by J.B. Kennedy, Gordon and Breach Science Publishers, New York, 1987.
- [3] K. Otsuka, H. Sakamoto and K. Shimizu, *Scripta Metall.* 9 (1975) p.491.
- [4] V. Novák, J. Malimánek and N. Zárubová, *Mater. Sci. Eng. A* 191 (1995) p.193.
- [5] K. Otsuka, H. Sakamoto and K. Shimizu, *Scripta Metall.* 10 (1976) p.983.
- [6] P. Šittner, K. Hashimoto, M. Kato and M. Tokuda, *Scripta Mater.* 48 (2003) p.1153.
- [7] X. Zhang, Q. Sun and S. Yu, *J. Mech. Phys. Solids* 48 (2000) p.2163.
- [8] P. Šittner, V. Novák and N. Zárubová, *Int. J. Mech. Sci.* 40 (1998) p.159.
- [9] P. Šittner and V. Novák, *Int. J. Plast.* 16 (2000) p.1243.
- [10] K. Otsuka and C.M. Wayman, *Shape Memory Materials*, Cambridge University Press, London, 1998.
- [11] M. Fremont and S. Miyazaki, *Shape Memory Alloys*, Springer, New York, 1996.
- [12] A.L. McKelvey and R.O. Ritchie, *Phil. Mag. A* 80 (2000) p.1759.
- [13] D. Wan and K. Komvopoulos, *J. Mater. Res.* 20 (2005) p.1606.
- [14] X.-G. Ma and K. Komvopoulos, *J. Mater. Res.* 20 (2005) p.1808.
- [15] H.-S. Zhang and K. Komvopoulos, *J. Mater. Sci.* 41 (2006) p.5021.
- [16] Y. Liu, Z.L. Xie, J. Van Humbeeck and L. Delaey, *Acta Mater.* 47 (1999) p.645.
- [17] C. Picornell, J. Pons and E. Cesari, *Acta Mater.* 49 (2001) p.4221.
- [18] H.-S. Zhang and K. Komvopoulos, *J. Mater. Res.* 22 (2007) p.994.
- [19] P. Thamburaja and L. Anand, *Acta Mater.* 51 (2003) p.325.
- [20] N. Abdullah, O. Kastner, I. Müller, A. Musolff, H. Xu and G. Zak, *Int. J. Non-Linear Mech.* 37 (2002) p.1263.
- [21] R. Gastien, C.E. Corbellani, M. Sade and F.C. Lovey, *Scripta Mater.* 50 (2004) p.1103.
- [22] J. Font, E. Cesari, J. Muntasell and J. Pons, *Mater. Sci. Eng. A* 354 (2003) p.207.
- [23] C. Picornell, J. Pons and E. Cesari, *Mater. Sci. Eng. A* 378 (2004) p.222.
- [24] D.-N. Fang, W. Lu and K.-C. Hwang, *Metall. Mater. Trans.* 30A (1999) p.1933.
- [25] J.M. McNaney, V. Imbeni, Y. Jung, P. Papadopoulos and R.O. Ritchie, *Mech. Mater.* 35 (2003) p.969.
- [26] T.W. Duerig, K.N. Melton, D. Stöckel and C.M. Wayman, *Engineering Aspects of Shape Memory Alloys*, Butterworth-Heinemann, London, 1990.
- [27] Y. Aydogdu, A. Aydogdu and O. Adiguzel, *J. Mater. Process. Tech.* 123 (2002) p.498.
- [28] N. Tamura, H.A. Padmore and J.R. Patel, *Mater. Sci. Eng. A* 399 (2005) p.92.
- [29] N. Tamura, A.A. MacDowell, R. Spolenak, B.C. Valek, J.C. Bravman, W.L. Brown, R.S. Celestre, H.A. Padmore, B.W. Batterman and J.R. Patel, *J. Synchrotron Radiat.* 10 (2003) p.137.
- [30] W.J. Choi, T.Y. Lee, K.N. Tu, N. Tamura, R.S. Celestre, A.A. MacDowell, Y.Y. Bong and L. Nguyen, *Acta Mater.* 51 (2003) p.6253.
- [31] M.R. Daymond, M.L. Young, J.D. Almer and D.C. Dunand, *Acta Mater.* 55 (2007) p.3929.
- [32] W.W. Schmahl, J. Khalil-Allafi, B. Hasse, M. Wagner, A. Heckmann and Ch. Somsen, *Mater. Sci. Eng. A* 378 (2004) p.81.
- [33] H. Miyamoto, T. Taniwaki, T. Ohba, K. Otsuka, S. Nishigori and K. Kato, *Scripta Mater.* 53 (2005) p.171.
- [34] S. Besseghini, F. Stortiero, G. Carcano, E. Villa, L. Mancini, G. Tromba, F. Zanini, F. Montanari and G. Airoldi, *Mater. Sci. Eng. A* 378 (2004) p.125.
- [35] A.S. Paula, J.H.P.G. Canejo, K.K. Mahesh, R.J.C. Silva, F.M. Braz Fernandes, R.M.S. Martins, A.M.A. Cardoso and N. Schell, *Nucl. Instrum. Meth. Phys. Res. B* 246 (2006) p.206.

- [36] S.W. Robertson, A. Mehta, A.R. Pelton and R.O. Ritchie, *Acta Mater.* 55 (2007) p.6198.
- [37] A. Mehta, X.-Y. Gong, V. Imbeni, A.R. Pelton and R.O. Ritchie, *Adv. Mater.* 19 (2007) p.1183.
- [38] W. Huang, *Mater. Des.* 23 (2002) p.11.
- [39] E. Patoor, D.C. Lagoudas, P.B. Entchev, L.C. Brinson and X. Gao, *Mech. Mater.* 38 (2006) p.391.
- [40] N. Siredey, E. Patoor, M. Berveiller and A. Eberhardt, *Int. J. Solids Struct.* 36 (1999) p.4289.
- [41] O. Matsumoto, S. Miyazaki, K. Otsuka and H. Tamura, *Acta Metall.* 35 (1987) p.2137.